Double-Sided Symmetrical and Crossed Emitter Crystalline Silicon Solar Cells With Heterojunctions for Bifacial Applications

Jyi-Tsong Lin, *Senior Member, IEEE*, Chung-Tse Lee, Wen-Hao Chen, Steve W. Haga, Yu-Yan Hu, and Kon-Yu Ho

***Abstract*—In this paper, we propose symmetrical and crossed bifacial crystalline silicon solar cells with heterojunctions employing a double-sided emitter, for use in environments with ambient light. We perform real measurement-based simulation analysis by using Silvaco TCAD Atlas. At an albedo level of 30%, our symmetrically structured solar cell achieves a 47.42 mA/cm^2 short-circuit current (J_{sc}) and a 29.72% conversion efficiency (η), due to the double-sided emitter's large area. These J_{sc} and η values are, respectively, 14.2% and 16.1% better than for a conventional Interdigitated Back Contact (IBC) [1]. The crossed structure obtains an 84.34% fill factor (FF) and a 29.81% conversion efficiency, due to its surrounding electric field. Conversion efficiency is increased by 16.4% compared with a conventional IBC solar cell [1]. Also, conversion efficiencies for the symmetrical and crossed bifacial SHJs are increased by 11.60% and 11.94%, respectively, compared with the state-of-the-art IBC solar cells [2].**

***Index Terms*—Bifacial, heterojunction with intrinsic thin-layer (HIT), interdigitated back contact (IBC), solar cell.**

I. Introduction

INTERDIGITATED Back Contact (IBC) solar cells are one of the most efficient Si devices for converting sunlight into electricity [1], [2]. The IBC's heterojunction of a hydrogenated amorphous silicon thin film to a crystalline substrate has fewer dangling bonds and better interface quality, leading to a higher open-circuit voltage V_{oc} [3]. The short-circuit current is also improved by avoiding optical loss due to moving the amorphous thin film, the Transparent Conducting Oxide (TCO) layer, and the metal from the front of the wafer to the back. An antireflection layer can enhance the light trapping ability [4]. Thick metal contacts decrease resistance and increase the fill factor (FF) [5]. According to the above reasons, IBC solar cells have been developed with high open-circuit voltage (0.74 V), short-circuit current (42.5 mA/ cm^2), and FF (84.65%), which all leads to a high conversion efficiency (26.63%) [2].

In order to reduce optical loss, the conventional IBC solar cell moved the metal and the depletion region to the back side. In consequence, however, some carriers are lost before reaching the back-side depletion region, particularly if the minority carrier diffusion length is much less than the cell thickness. The conventional monofacial solar cell also has the problem that its maximum output power occurs during a narrow portion of the daytime, while energy storage systems have limitations [6]. Another challenge is that conventional monofacial electrodes cannot use reflected light, while the heat thereby generated decreases solar cell performance [7].

We address the above problems through a bifacial crystalline silicon solar cell with a heterojunction and double-sided emitters. We propose two versions of the silicon solar cells with heterojunctions (SHJ) device, symmetrical and crossed. These two new SHJ structures each improve the recombination problem, the maximum output power problem and the thermal degradation problem, while retaining a high open-circuit current, a high FF, and a high conversion efficiency performance.

An extra 20% to 30% albedo is typically available to solar cells, due to reflected and scattered light from the ground or clouds [8]. A bifacial SHJ structure helps to convert this extra light. Moreover, the bifacial SHJ structure can have two peak output times per day, if mounted appropriately, unlike the monofacial structure [3], [9]. An additional advantage of the bifacial SHJ structure is that the maximum output power benefits from the decreased working temperature resulting from the lessened infrared absorption in the absence of aluminum back metallization [10]. The temperature coefficient of a bifacial SHJ structure is therefore better than a monofacial SHJ structure. With albedo light, photons not only are gathered at the front surface but also at the back surface. The double-sided emitter reduces the path distance that minority carriers have to travel, allowing for a reduced recombination rate. By considering both symmetrical and crossed placements of these double-sided emitters, we observe the effect of altering that path.

When incident light arrives at the cell surface, it is absorbed and the solar cell generates electron–hole pairs. In a conventional monofacial SHJ cell [3], majority carriers must then traverse the whole thickness of the substrate before reaching the back surface field (BSF). In contrast, our symmetrical SHJ

Manuscript received August 14, 2017; revised December 11, 2017 and December 20, 2017; accepted December 30, 2017. Date of publication February 5, 2018; date of current version February 16, 2018. This work was supported by the Ministry of Science and Technology of Taiwan under Contact MOST-104-2221-E-110-029-MY3. *(Corresponding author: Jyi-Tsong Lin.)*

J.-T. Lin, C.-T. Lee, W.-H. Chen, Y.-Y. Hu, and K.-Y. Ho are with the Department of Electrical Engineering, National Sun Yat-Sen University, Kaohsiung 80424, Taiwan (e-mail: jtlin@ee.nsysu.edu.tw; th112696@gmail.com; poin.ssetia@gmail.com; ggyybiggo@gmail.com; s830723@gmail.com).

S. W. Haga is with the Department of Computer Science and Engineering, National Sun Yat-sen University, Kaohsiung 80424, Taiwan (e-mail: stevewhaga@cse.nsysu.edu.tw).

Color versions of one or more of the figures in this paper are available online at http://ieeexplore.ieee.org.

Digital Object Identifier 10.1109/JPHOTOV.2018.2790798

2156-3381 © 2018 IEEE. Personal use is permitted, but republication/redistribution requires IEEE permission.
See http://www.ieee.org/publications_standards/publications/rights/index.html for more information.

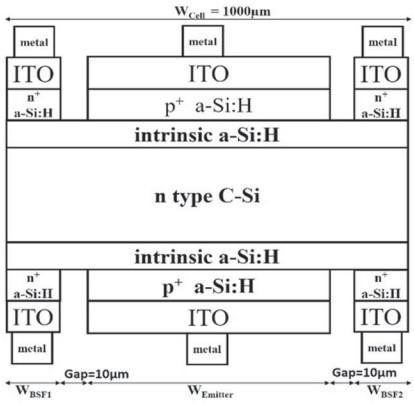

$W_{BSF1+BSF2} : W_{Emitter}$	1:8	1:9	1:10	1:11	1:12	1:13
$W_{BSF1+BSF2}$ (μm)	108	98	90	82	76	70
$W_{Emitter}$ (μm)	872	882	890	898	904	910

Fig. 1. Schematic diagram of the symmetrical version of our double-sided emitter crystalline silicon solar cell with a heterojunction . The symetry property refers to the fact that the p^+ (and n^+) regions are horizontally alligned (i.e., the ITOs at the center-top and center-bottom both touch p+ regions). The double-sided emitter layers lead to an improved energy boost.

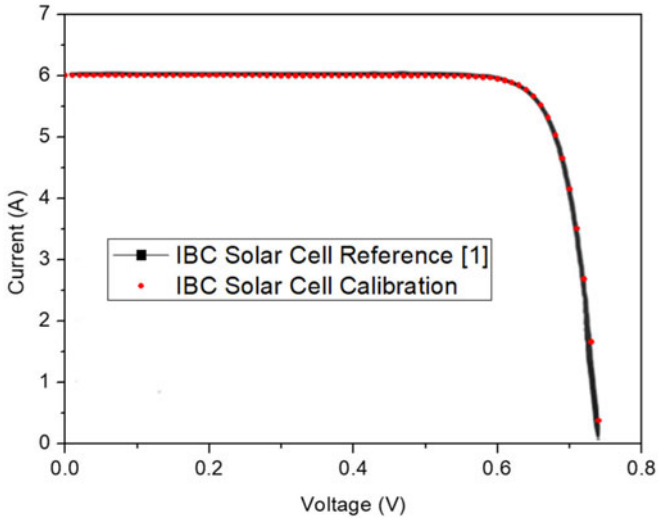

Fig. 2. Comparison of the physically measured *I–V* curve of the IBC solar cell [1] and the calibrated simulation curve of that cell.

structure allows the generated electron–hole pairs to separate and move to their respective optimal regions. The crossed version of the SHJ structure has additional surrounding electric fields that can further enhance carrier mobility and decrease carrier recombination.

Fig. 1 shows the structure of our double-sided symmetrical emitter crystalline silicon solar cell with a heterojunction. This structure preserves as high quality an amorphous silicon layer as the hydrogenated one in an IBC solar cell, with a good temperature coefficient. Moreover, the larger depletion region area obtained by double-sided emitters allows for increased carrier collection.

II. Device Simulation and Parameter Calibration

In this paper, the solar cell was operated under a global standard solar spectrum (AM 1.5G) illumination with a total incident power density of 100 mW/cm^2. The light intensity was calculated for each wavelength from 300 to 1200 nm [12]. Simulations were performed using Silvaco Atlas with the ray-tracing model.

The optical constants values were obtained in an initial calibration step. By taking the geometry and process-related parameters presented in the Panasonic reference paper [1] along with the defect parameters presented in [13], initial calibration could be performed to ensure that the simulation results are consistent with the reported measurements [1]. The models, assumptions, and their related parameters were carefully checked and adjusted to minimize the differences to the reported values. Fig. 2 compares the measured *I–V* curve with the calibrated simulation curve of the IBC solar cell. The close agreement of the two curves in Fig. 2 ensures the authenticity of the simulation.

The calibrated parameters are shown in Table I. By using these values, all of our extended simulations are based on measurements and the same processes as discussed in the calibration reference [1].

TABLE I
Device Parameters* Used in All Our Simulations

Parameters		n-c-Si	i-a-Si:H	p^+-a-Si:H	n^+-a-Si:H
Energy gap (eV)		1.12	1.8	1.8	1.8
Donor doping density (cm^{-3})		1×10^{16}	0	0	1×10^{19}
Acceptor doping density (cm^{-3})		0	0	5×10^{19}	0
Electron mobility (cm^2/Vs)		1500	20	20	20
Hole mobility (cm^2/Vs)		500	0.1	0.1	0.1
Electron life time (s)		7×10^{-4}	1×10^{-5}	1×10^{-5}	1×10^{-5}
Hole life time (s)		7×10^{-4}	1×10^{-6}	1×10^{-6}	1×10^{-6}
Effective valence band density (cm^{-3})		1.04×10^{19}	2.5×10^{20}	2.5×10^{20}	2.5×10^{20}
Effective conduction band density (cm^{-3})		2.8×10^{19}	2.5×10^{20}	2.5×10^{20}	2.5×10^{20}
Permittivity (F/m)		11.9	11.9	11.9	11.9
Affinity (eV)		4.05	3.8	3.8	3.8
Thickness		150 (μm)	10 (nm)	10 (nm)	10 (nm)
Conduction tail states [13]	$N_A^{c-\text{tail}}$	N/A	1×10^{18} cm^{-3}	1×10^{21} cm^{-3}	1×10^{21} cm^{-3}
	$E_A^{c-\text{tail}}$	N/A	0.06 eV	0.07 eV	0.07 eV
Valence tail states [13]	$N_D^{v-\text{tail}}$	N/A	1×10^{18} cm^{-3}	1×10^{21} cm^{-3}	1×10^{21} cm^{-3}
	$E_D^{v-\text{tail}}$	N/A	0.09 eV	0.12 eV	0.12 eV
Acceptor-like dangling bond states [13]	N_A^{db}	N/A	1×10^{16} cm^{-3}	1×10^{19} cm^{-3}	1×10^{19} cm^{-3}
	E_A^{db}	N/A	1.1 eV	1.3 eV	0.7 eV
	δ_A^{db}	N/A	0.15 eV	0.2 eV	0.2 eV
Donor-like dangling bond states [13]	N_D^{db}	N/A	1×10^{16} cm^{-3}	1×10^{19} cm^{-3}	1×10^{19} cm^{-3}
	E_D^{db}	N/A	0.9 eV	1.1 eV	0.45 eV
	δ_D^{db}	N/A	0.15 eV	0.2 eV	0.2 eV

*These parameters are calibrated from the real fabrication of an IBC cell [1].

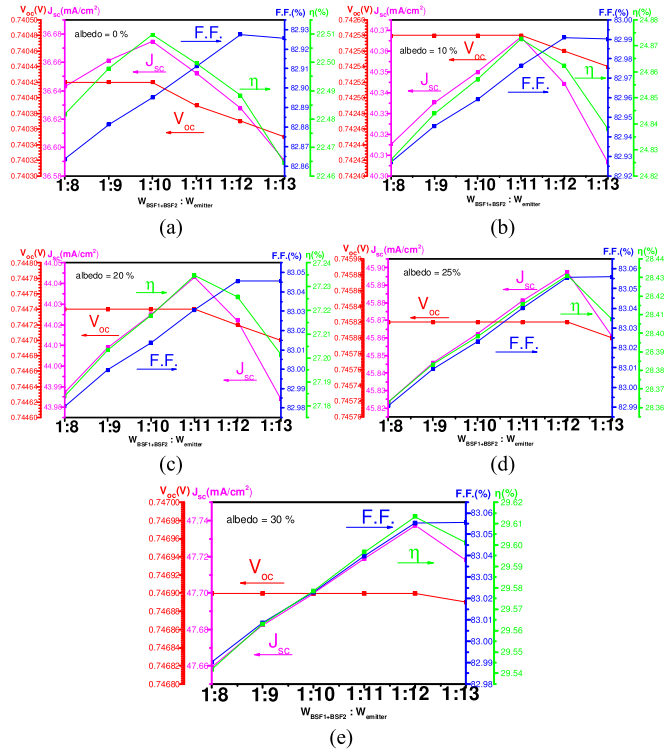

Fig. 3. Influence of the $W_{\mathrm{BSF1+BSF2}}$: W_{emitter} ratio with respect to the J_{sc}, V_{oc}, FF, and η in monofacial and bifacial SHJs with different intensities of albedo. (a) Monofacial condition. $W_{\mathrm{BSF1+BSF2}}$: W_{Emitter} = 1: 10 has better η than other ratios. (b)–(e) Bifacial symmetrical condition with 10%, 20%, 25%, and 30% albedo. As the intensity of albedo increases, larger emitter widths have better η.

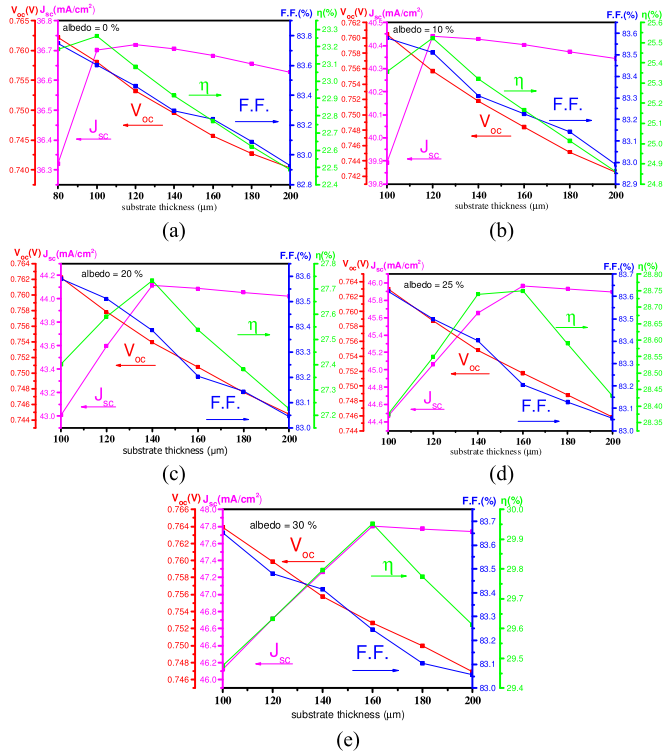

Fig. 4. Influence of substrate thickness to the J_{sc}, V_{oc}, FF, and η. (a) Monofacial condition, where a substrate thickness of 100 μm gives the best η. (b)–(e) Bifacial symmetrical condition with 10%, 20%, 25%, and 30% albedo. As the intensity of albedo increases, the optimal substrate thickness increases.

III. Results and Discussion

Calibrated parameter simulation clarifies the advantages of bifacial SHJ structures. We evaluate the effects of the width ratio $W_{\mathrm{BSF1+BSF2}}$: W_{emitter} (i.e., the summation of BSF widths compared with the emitter width), and the substrate thickness. We also measure the photogeneration rate, the electric field direction, and the electron hole current density.

Fig. 3 shows the influence of $W_{\mathrm{BSF1+BSF2}}$: W_{Emitter} with respect to the short-circuit current density (J_{sc}), open-circuit voltage (V_{oc}), FF, and conversion efficiency (η), at different albedo levels. The conversion efficiency is dominated by the short-circuit current density. In Fig. 3(a), a ratio of 1: 10 has the best conversion efficiency. This agrees with the previous work [14]. Unlike that previous work, however, we also look at other albedo conditions. Fig. 3(b) and (c) give the results for 10% and 20% albedo, where a ratio of 1: 11 yields the best conversion efficiency. Fig. 3(d) and (e) show that at albedos of 25% and 30% the optimal ratio is 1:12.

Thus, as the albedo intensifies, the emitter should be widened for optimal conversion efficiency. This is due to the differences in the respective collection and absorption abilities of minority carriers and photons. Just as some photons coming down from sunlight will pass through to reach the rear-side substrate, so also some reflected light coming back up will pass through and reach the surface of front-side substrate. When these photons convert into electron–hole pairs, more current is generated than in the monofacial condition. Increasing the emitter width can enhance the collection ability of the holes. But the collection ability of electrons wouldn't decrease as much due to a narrower BSF width, because the n-type substrate's excess electrons have about three times greater mobility than holes do. Since albedos of 20% to 30% are typical [8], we chose 1:12 as the $W_{\mathrm{BSF1+BSF2}}$: W_{Emitter} ratio for our double-sided symmetrical emitter structure.

Fig. 4 shows the influence of substrate thickness on J_{sc}, V_{oc}, FF, and conversion efficiency. Fig. 4(a) shows that, in the monofacial condition, a thickness of 100 μm gives the best conversion efficiency, due to the short minority transport distance [15]. But, as the albedo increases, so also does the optimal thickness: 120 μm at 10% albedo, 140 μm at 20% albedo, 150 μm at 25% albedo, and 160 μm at 30% albedo. The reason for this thickness increase is related with the quantities of photons and the double-sided emitter layer. Although a thicker substrate means that it can trap more photons, it also means that some minority carriers will need to travel farther and will have more chance to recombine and will thereby decrease the open-circuit voltage and the fill factor. Whereas a conventional monofacial solar cell only has an emitter layer on one side, our double-sided emitter allows the holes and electrons to move only half as far to reach the anode or cathode. The short-circuit current increases when the substrate thickness become thicker. In order to achieve the best conversion efficiency with 30% albedo, we choose 160 μm as our substrate thickness.

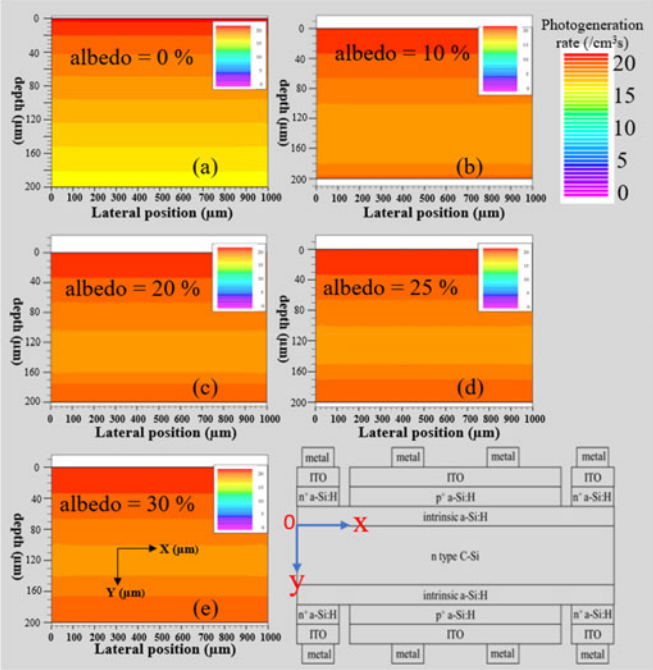

Fig. 5. Photogeneration profiles for different intensities of albedo. (a) Monofacial condition. The vertical range up to 100 μm accounts for most of the photogeneration. (b)–(e) Bifacial symmetrical condition with 10%, 20%, 25%, and 30% albedo. The higher photogeneration regions are: (0–100 μm, 180–200 μm), (0–100 μm, 160–200 μm), (0–100 μm, 150–200 μm), and (0–100 μm, 140–200 μm), respectively. A 10% increase in the albedo increases the height of the important region by about 20 μm.

Fig. 5 shows the photogeneration profiles for 200 μm of substrate. Comparing Fig. 5(a)–(e), the number of photons at the bottom side in 200 μm's substrate is an obvious consequence of the albedo level (i.e., the amount of light coming from the bottom). The optimal thickness is also suggested by the figure. For Fig. 5(a), photogeneration is low after about 100 μm. This agrees with what Fig. 4(a) had shown: that 100 μm was best for the monofacial device. In Fig. 5(b)–(e), we find that an albedo increase of 10% tends to extend the high-photogenerating portions of the substrate by about 20 μm. At 30% albedo, for example, the high generation regions are from 0 to 100 μm and from 40 to 200 μm. This total of 160 μm is in agreement with what Fig. 4(e) had found. Compared with Fig. 4, the insight of Fig. 5 is that the albedo-induced increase in photogeneration largely occurs at the bottom of the substrate.

Fig. 6 shows our second structure, the double-sided crossed emitter crystalline silicon solar cell with heterojunction. The only difference with Fig. 1 is that the p^+ and n^+ regions are crossed. The large area of the front emitter allows the depletion region to absorb more photons. This crossing means that each p^+ region will have an n^+ region on the opposite side as well as on both sides, thereby forming a surrounding electric field. This surrounding electric field causes the solar cell to have a low series resistance and a low recombination rate. This improves the V_{oc} and the FF of the cell.

Our simulations find that this structure has better conversion efficiency for albedo intensities below 30%. At these low albedos, the bifacial solar cell does not need much emitter width

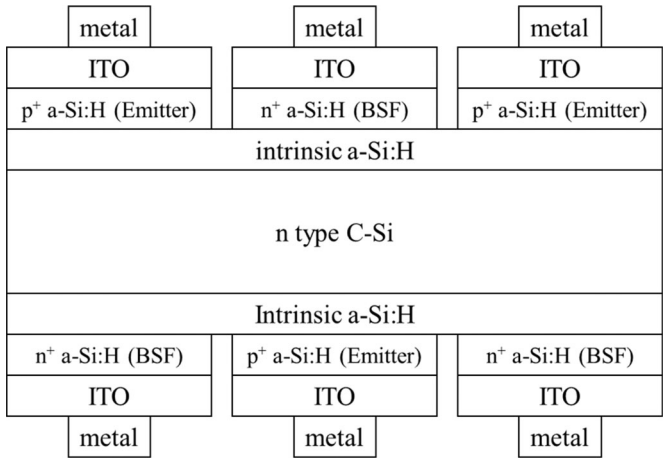

Fig. 6. Schematic diagram of our double-sided crossed emitter crystalline silicon solar cell with heterojunction. As compared with the symetrical version, the p^+ and n^+ regions are both crossed. This can form a surrounding electric field, which can allow the solar cell to have a low series resistance circuit and recombination rate. This can improve the V_{oc} and FF.

on the bottom surface, because fewer photons reach this region. In fact, even at high albedos, the best conversion efficiency still required relatively narrower back-side emitters, when compared to the width of the top-side emitters. This makes sense for three reasons:

1) less light reaches the back surface, so the emitters do not need to be as wide as at the top;
2) the space thereby saved allows for wider bottom BSF regions to enhance carrier mobility;
3) the top-side emitter can compensate for the back-side reduction (we tested changing the bottom emitter to a BSF, and found that the top emitter did indeed collect more minority carriers).

Fig. 7 shows the electric field direction for the crossed version of our bifacial device. Fig. 7(a)–(d) gives the direction of the electric field in the p–n gap of our solar cell. Fig. 7(e) is the schematic diagram of the electric field. As can be seen, the crossed placement produces a surrounding electric filed that reduces the chance of recombination, so as to significantly increase V_{oc} and the FF.

A back-surface field is generally used in conventional silicon solar cells to push minority carriers away from the back-surface field region [15]. So, we also use this function to increase the mobility of minority carriers. Through this surrounding electric field, the FF of the crossed structure reaches 84.34%. In order to prove the electric field is useful, Fig. 8 shows the hole current density of our crossed SHJ structure. Due to the surrounding electric field, the holes are pushed near the emitter layers, so there is high hole current density near those layers.

Fig. 9 shows the difference between a conventional heterojunction with intrinsic thin-layer (HIT) solar cell with a monofacial and bifacial structures [3]. The most important difference is the metal being separated on the rear side. This was done so as to allow some light to enter the solar cell from the bottom surface, although this also does reduce the amount of light from above that gets reflected back through the device.

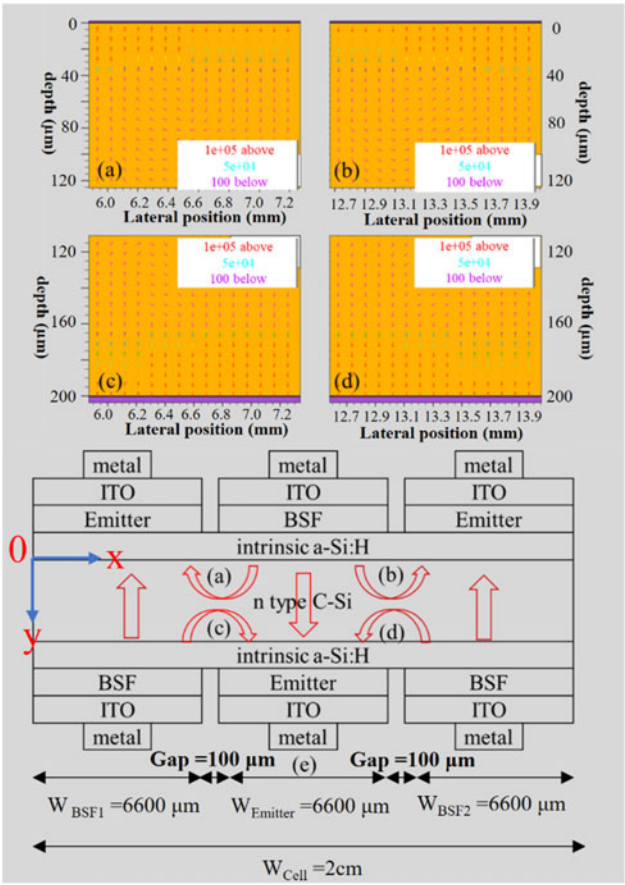

Fig. 7. Electric field direction of our double-sided crossed emitter crystalline silicon solar cell with heterojunction. (a)–(d) The electric field in the p-n gap. (e) Schematic diagram of the electric field in the crossed-emitter solar cell. The crossed placement causes each emitter layer to be across from a BSF layer, and also in between BSF layers to the left and right. This placement forms a surrounding electric field for minority carriers.

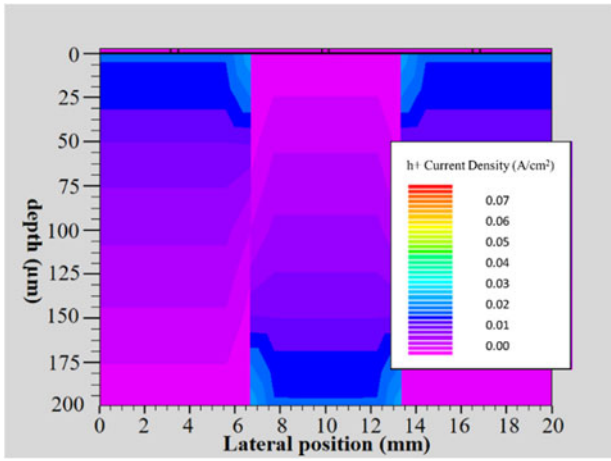

Fig. 8. Hole current density of the crossed structure. There is a high hole current density near the emitter layers, due to the surrounding electric field, as in Fig. 7.

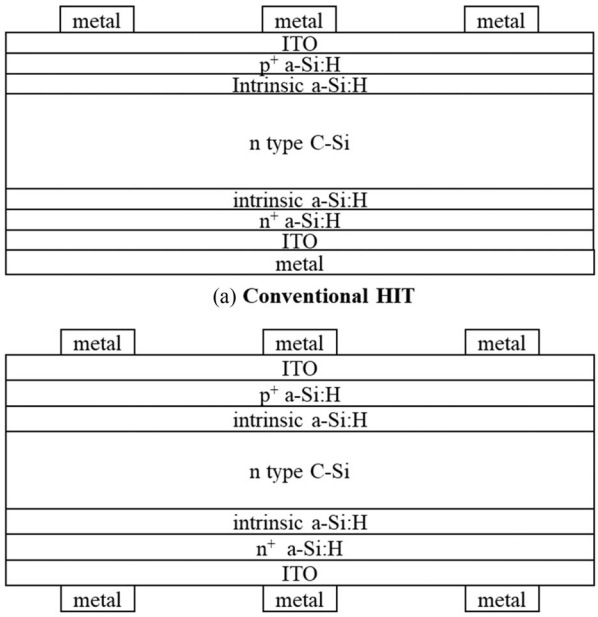

Fig. 9. Change of conventional HIT solar cell from (a) standard mono-facial [3] to (b) standard bifacial.

Fig. 10 shows the *I–V* curves between the conventional standard HIT solar cell structure and the standard Bifacial Heterojunction with Intrinsic Thin-layer (Bi-HIT) solar cell, which are SHJs. The conventional HIT solar cell had already been calibrated by Silvaco Atlas [3]. We then separated the bottom-side metal and simulated our new standard Bi-HIT structure. The conventional HIT solar cell has better short-circuit current due to the nearly full reflection of light due to the full coverage of the metal layer on the bottom side.

Fig. 11 shows the conversion efficiency of a standard bifacial HIT (Bi-HIT) solar cell, a symmetrical and a crossed SHJ structure, at different albedo intensities. The standard Bi-HIT solar cell has its best conversion efficiency in the monofacial condition, due to the larger emitter at the top surface. As described above, most of the photons are captured near the top surface; in the monofacial condition, the larger emitter at the front surface reduces the distance that minority carriers need to travel and their recombination rate. However, the SHJ structures with double-sided emitters have better conversion efficiency when the albedo rises above 20%.

Fig. 12 shows the energy boost of the Bi-HIT solar cell, the symmetrical and the crossed SHJ structures, for different albedos. From this graph, we can understand that our bifacial structure has three advantages. First, it has large emitters. Having large emitters reduces the travel distance and recombination rate of minority carriers. With an increase of albedo, there are more photons available, so a larger emitter can collect more minority carriers. Second, it has emitters on both sides. By using double-sided emitters, the minority carriers which gather near the bottom surface can be directly collected by the emitter. Third, it has a sufficiently thick silicon substrate. Although a thicker substrate would absorb more photons, it would also have more recombinations. So the optimal substrate should be thick enough to capture the photons, but not so thick as to lose the carriers. And since the number of available photons increases with the albedo, this means that the optimal substrate

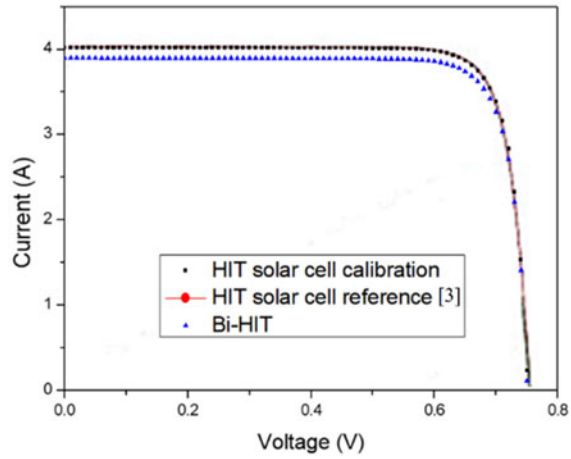

Fig. 10. *I–V* curves between the conventional HIT solar cell structure [3] and the Bi-HIT solar cell. The conventional HIT solar cell has better short-circuit current than the Bi-HIT solar cell because more light is reflected from the metal layer since it fully covers the bottom side.

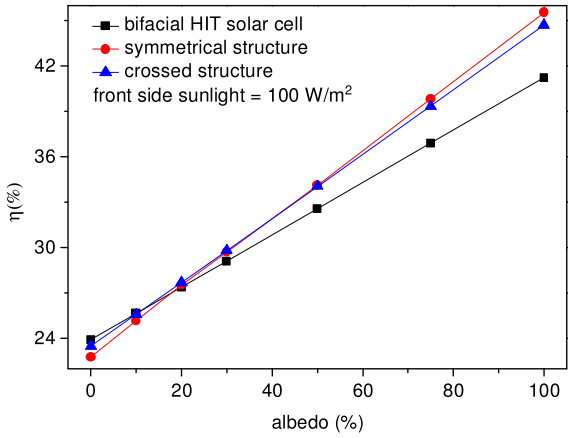

Fig. 11. Conversion efficiencies of a standard Bi-HIT solar cell, a symmetrical, and crossed SHJ structures, at different albedo intensities. The intensity of sunlight from the front side was set to 100 mW/ cm^2 and the albedo was varied from 0% to 100%. The SHJ structures with double-sided emitter have better conversion efficiency when the albedo intensity exceeds 20%.

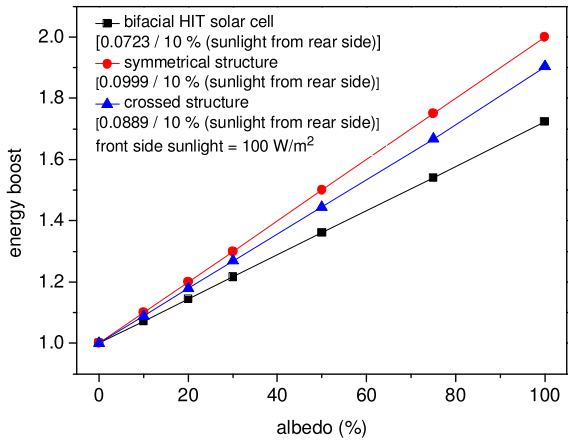

Fig. 12. Energy boost of a Bi-HIT solar cell, a symmetrical, and a crossed SHJ structure, at different albedo intensities. The symmetrical structure has the best energy boost as long as there is some albedo.

TABLE II
COMPARISON OF BIFACIAL HIT, SYMMETRICAL SHJ STRUCTURE, AND CROSSED SHJ STRUCTURE

Solar Cell	Bifacial ratio (%)	J_{sc} (mA/cm^2)	V_{oc} (V)	FF (%)	η (%)
Bi-HIT	0	38.29	0.75	83.25	23.92
[Fig. 9(b)]	30	46.12	0.75	83.65	29.10
	100	64.77	0.76	83.67	41.23
Symmetrical	0	36.69	0.75	83.26	22.77
(Fig. 1)	30	47.42	0.75	83.11	29.72
	100	71.50	0.77	82.91	45.54
Crossed	0	36.94	0.75	84.35	23.50
(Fig. 6)	30	46.41	0.76	84.34	29.81
	100	68.53	0.77	84.31	44.69

thickness also increases. For our structure, when the substrate thickness is 160 μm, our solar cell has the best η. Table II shows also the benchmark comparison among the Bi-HIT, symmetrical structure and crossed structure.

IV. CONCLUSION

We have developed symmetrical and crossed bifacial crystalline silicon solar cells with heterojunctions by using double-sided emitters. As a result, we found that our bifacial SHJ solar cells possess three unique characteristics that boost conversion efficiency: large emitters, bifacial emitters, and an appropriate substrate thickness. Through these, the bifacial symmetrical emitter solar cell exhibits a 47.42 mA/ cm^2 short-circuit current density and a 29.72% conversion efficiency for a 30% albedo. Also, the bifacial crossed solar cell achieves a 29.81% conversion efficiency and an 84.34% fill factor, due to the electric field surrounding its emitters.

Despite these positive results, it should be noted that the widths of the BSF regions might be too narrow for current commercial mass production. But as scaling improves in the future, the proposed device could find application in an integrated photoelectronics single-chip systems.

REFERENCES

[1] K. Masuko *et al.*, "Achievement of more than 25% conversion efficiency with crystalline silicon heterojunction solar cell," *IEEE J. Photovolt.*, vol. 4, no. 6, pp. 1433–1435, Nov. 2014, doi: 10.1109/ JPHOTOV.2014.2352151.

[2] K. Yoshikawa *et al.*, "Exceeding conversion efficiency of 26% by heterojunction interdigitated back contact solar cell with thin film Si technology," *Sol. Energy Mater. Sol. Cells*, vol. 173, pp. 37–42, 2017, doi: 10.1016/j.solmat.2017.06.024.

[3] M. Taguchi *et al.*, "24.7% record efficiency HIT solar cell on thin silicon wafer," *IEEE J. Photovolt.*, vol. 4, no. 1, pp. 96–99, Jan. 2014, doi: 10.1109/JPHOTOV.2013.2282737.

[4] B. Shu *et al.*, "Design of anti-reflection coating for surface textured interdigitated back contact silicon hetero junction solar cell," in *Proc. 38th IEEE Photovoltaic Spec. Conf.*, Jun. 2012, pp. 002258–002262, doi: 10.1109/PVSC.2012.6318047.

[5] P. Magnone, M. Debucquoy, D. Giaffreda, N. Posthuma, and C. Fiegna, "Understanding the influence of busbars in large-area IBC solar cells by distributed SPICE simulations," *IEEE J. Photovolt.*, vol. 5, no. 2, pp. 552–558, Mar. 2015, doi: 10.1109/JPHOTOV.2015.2392939.

[6] J. Rodriguez, "Bifacial solar cells – the two sides of the story," May 2015. [Online]. Available: https://www.solarchoice.net.au/blog/news/bifacial-solar-cells-the-two-sides-of-the-story-050515
[7] F. Reis *et al.*, "Modeling the effects of inhomogeneous irradiation and temperature profile on CPV solar cell behavior," *IEEE J. Photovolt.*, vol. 5, no. 1, pp. 112–122, Jan. 2015, doi: 10.1109/JPHOTOV.2014.2358080.
[8] J. L. Hernández *et al.*, "High efficiency silver-free heterojunction silicon solar cell," *Jpn. J. Appl. Phys.*, vol. 51, no. 10s, pp. 3644–3648, Oct. 2012, doi: 10.1143/JJAP.51.10NA04.
[9] R. Kopecek *et al.*, "Bifaciality: One small step for technology, one giant leap for kWh cost reduction," *Photovolt. Int.*, vol. 26, Jan. 2015. [Online]. Available: https://www.pv-tech.org/technical-papers/bifaciality-one-small-step-for-technology-one-giant-leap-for-kwh-cost-reduc
[10] R. Guerrero-Lemus, R. Vega, T. Kim, A. Kimm, and L. E. Shephard, "Bifacial solar photovoltaics—A technology review," *Renewable Sustain. Energy Rev.*, vol. 60, pp. 1533–1549, Jul. 2016. doi: 10.1016/j.rser.2016.03.041.
[11] Silvaco© "ATLAS User's Manual," Aug. 30, 2016. [Online]. Available: https://dynamic.silvaco.com/dynamicweb/jsp/downloads/DownloadManualsAction.do?req=silen-manuals&nm=atlas
[12] Y. Hayashi, D. Li, A. Ogura, and Y. Ohshita, "Role of i-aSi:H layers in aSi:H/cSi heterojunction solar cells," *IEEE J. Photovolt.*, vol. 3, no. 4, pp. 1149–1155, Oct. 2013. doi: 10.1109/JPHOTOV.2013.2274616.
[13] M. Filipič, F. Smole, and M. Topič, "Optimization of interdigitated back contact geometry in silicon heterojunction solar cell," in *Proc. 14th Int. Conf. Numer. Simul. Optoelectron. Devices*, Sep. 2014, pp. 161–162, doi: 10.1109/NUSOD.2014.6935406.
[14] C. Petti, B. Newman, R. Brainard, and J. Li, "Optimal thickness for crystalline silicon solar cells," *Twin Creek Technol.*, vol. 2, pp. 1–15, 2011, doi: 10.1109/JPHOTOV.2013.2274616.
[15] A. Rawat, M. Sharma, D. Chaudhary, S. Sudhakar, and S. Kumar, "Numerical simulations for high efficiency HIT solar cells using microcrystalline silicon as emitter and back surface field (BSF) layers," *Sol. Energy*, vol. 110, pp. 691–703, Dec. 2014, doi: 10.1016/j.solener.2014.10.004.

Jyi-Tsong Lin (M'96–SM'08) was born in Taiwan in 1959. He received the B.S. degree in physics from National Taiwan Normal University, Taipei, Taiwan, in 1982, the M.S. degree in electronics from National Chiao Tung University, Hsinchu, Taiwan, in 1984, and the Ph.D. degree in electronics and computer science from the University of Southampton, Southampton, U.K., in 1993.

He has been with the National Sun Yat-sen University, Kaohsiung, Taiwan, since 1984, where he is currently a Professor with the Department of Electrical Engineering. His research interests include the design and modeling of small-geometry SOI devices and the design of high-speed and low-power circuits of bulk and SOI MOSFETS. He was recently working on the development and process integration of nonclassical SOI, TFT nanodevices, TFET, solar cell, and one transistor memory.

Chung-Tse Lee received the B.S. degree in electrical engineering from National University of Kaoshiung, Kaoshiung, Taiwan in 2015. He is currently working toward the M.S. degree in electrical engineering at the National Sun Yat-sen University, Kaohsiung.

Wen-Hao Chen is currently working toward the M.S. degree in electrical engineering at the National Sun Yat-sen University, Kaohsiung, Taiwan.

Steve W. Haga received the Ph.D. degree in electrical engineering from the University of Maryland, College Park, MD, USA.

He is currently an Assistant Professor with the Department of Computer Science and Engineering, National Sun Yat-sen University, Kaohsiung, Taiwan. His current research interests include compiler optimizations for real-time systems and GPGPUs, computer architectures, and memory systems.

Yu-Yan Hu received the B.S. degree in electrical engineering from National Kaoshiung University of Applied Sciences, Kaoshiung, Taiwan, in 2015. He is currently working toward the M.S. degree in electrical engineering with the National Sun Yat-sen University, Kaohsiung.

Kon-Yu Ho is currently working toward the M.S. degree in electrical engineering with the National Sun Yat-sen University, Kaohsiung, Taiwan.